Journal of Materials Chemistry A

Accepted Manuscript

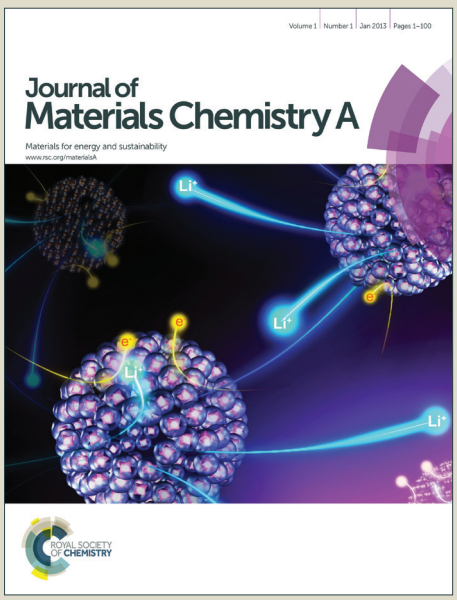

ROYAL SOCIETY OF CHEMISTRY

www.rsc.org/materialsA

Cite this: DOI: 10.1039/c0xx00000x

www.rsc.org/xxxxxx

ARTICLE TYPE

In situ light-assisted preparation of MoS_2 on graphitic C_3N_4 nanosheet for enhanced photocatalytic H_2 production from water

Hui Zhao, Yuming Dong,* Pingping Jiang,* Hongyan Miao, Guangli Wang, Jingjing Zhang

Received (in XXX, XXX) Xth XXXXXXXXX 20XX, Accepted Xth XXXXXXXXX 20XX

DOI: 10.1039/b000000x

MoS_2-decorated graphitic C_3N_4 (g-C_3N_4/MoS_2) photocatalysts were prepared by a simple and scalable in situ light-assisted method. In this process, the MoS_2 formed from the reduction of $[MoS_4]^{2-}$ by the photogenerated electrons and then in situ loaded on the electron outlet points of g-C_3N_4. The g-C_3N_4/MoS_2 composite was well characterized by X-ray diffraction (XRD), Fourier Transform infrared spectroscopy (FTIR), Raman spectroscopy (Raman), Transmission electron microcopy (TEM), Energy Dispersive X-Ray spectroscopy (EDX), and ultraviolet visible diffuse reflection spectroscopy (UV-DRS). The g-C_3N_4/MoS_2 photocatalysts showed a good photocatalytic H_2 evolution activity. When the loading amount of MoS_2 increased to 2.89 wt% (g-C_3N_4/MoS_2-2.89%), the highest H_2 evolution rate (252 μmol g^{-1} h^{-1}) was obtained. In addition, g-C_3N_4/MoS_2-2.89% presented stable photocatalytic H_2 evolution ability (no noticeable degradation of photocatalytic H_2 evolution was detected in 18 h) and good natural light driven H_2 evolution ability (the H_2 evolution rate was 320 μmol g^{-1} h^{-1}). A possible photocatalytic mechanism of MoS_2 cocatalyst on the improvement of the photocatalytic activity for g-C_3N_4 is proposed that MoS_2 can efficiently promote the separation of photogenerated electrons and holes of g-C_3N_4 consequently enhancing the H_2 evolution activity, which is supported by the photoluminescence spectroscopy and photoelectrochemical analyses.

1. Introduction

With increasing awareness of the importance of energy crisis and environmental pollution, the development of green renewable energy has been greatly promoted. Hydrogen is regarded as a potential fuel to solve the fossil fuel shortage problem and environmental issues. Photocatalytic water decomposition into hydrogen is a valuable approach to utilize solar energy, which is recognized as a green and promising way to produce clean energy.[1-3] During the past years, many photocatalysts have been developed, such as TiO_2, CdS and $Zn_xCd_{1-x}S$.[4-6] At the same time, various drawbacks, such as low visible-light adsorption ability and fast recombination rate of photogenerated electron-holes pairs, and high toxic for human health and harmful to the environment greatly limit practical application for solar hydrogen generation. To address these limitations, development of novel visible-light responsive photocatalysts with high efficiency and good durability has become a hot topic in the photocatalysis field.

As a novel metal-free polymer n-type semiconductor, layered C_3N_4 with a graphitic structure (g-C_3N_4) revealed good visible light absorption property (E_g = 2.7 eV) and photocatalytic stability for water splitting.[7-13] In comparison with the most studied semiconductor materials (e.g. TiO_2, CdS, $Zn_xCd_{1-x}S$), g-C_3N_4 combines the advantages of low cost, nontoxicity and visible-light activity. Hence, g-C_3N_4 should be a good candidate for photocatalytic solar energy conversation.[14] However, the photocatalytic activity of pure g-C_3N_4 is low due to its fast recombination of photogenerated electron-hole pairs. Cooperating g-C_3N_4 with cocatalyst has been proved to be an effective way to facilitate the charge separation of the photogenerated electron-hole pairs by lowering the activation barriers of water splitting.[15,16] To date, the reported cocatalysts are mainly noble metals Pt, Au and Pd,[17-19] which are rare and expensive. Accordingly, there is an increasing interest in introducing low-cost non-noble metal cocatalysts into g-C_3N_4.

Molybdenum sulfide (MoS_2) has emerged as a promising electrocatalyst due to its high activity, earth-abundant composition, low cost and robustness.[20,21] There have been reported studies on the modification of semiconductor with MoS_2 cocatalyst to accelerate the photocatalytic hydrogen evolution.[22-24] Hence, employing MoS_2 as an alternative cocatalyst for g-C_3N_4 in photocatalytic H_2 generation is very attractive. In this connection, the effective combination of g-C_3N_4 and MoS_2 is vital for quick transfer of electrons, which is among the keys for catalysis efficiency. Desirable g-C_3N_4/MoS_2 photocatalysts depend greatly on the preparation methods. Recently, thin-layered MoS_2 was cooperated with g-C_3N_4 by a thermal deposition process and high photocatalytic activity for H_2 production was obtained.[25] MoS_2 loaded g-C_3N_4 prepared via an impregnation method has been found to be highly efficient in H_2 production.[26,27] MoS_2 decorated g-C_3N_4 through a hydrothermal preparation exhibited a high photocatalytic activity and good stability.[28] However, among these methods, the thermal

deposition process involved a relatively harsh preparation condition of high temperature and high pressure and toxic H_2S gas used as co-precursor; In the impregnation method, MoS_2 was first prepared under the condition of high temperature and high pressure, and the following heated treatment was necessary for combination of MoS_2 and g-C_3N_4; In the hydrothermal preparation, complicated reaction steps were necessary and toxic $NH_2OH{\cdot}HCl$ was needed to take part in the reaction. Obviously, these methods are complicated, environmentally harmful or energy-hungry. In addition, the connective point between MoS_2 and g-C_3N_4 is difficult to control by these methods. Therefore, to design novel and facile preparation strategy for g-C_3N_4/MoS_2 hybrid photocatalysts is still urgent and of great significance.

Herein, MoS_2 modified g-C_3N_4 (g-C_3N_4/MoS_2) hybrid photocatalysts were prepared by a simple and scalable in situ light-assisted method in photocatalytic H_2 evolution system, where $(NH_4)_2[MoS_4]$ was used as the source of MoS_2. In this process, the MoS_2 formed from the reduction of $[MoS_4]^{2-}$ by the photogenerated electrons and then in situ loaded on the electron outlet points of g-C_3N_4. The formation method of MoS_2 decided that the obtained structure is favorable for transfer of photogenerated electrons, which could be helpful for highly robust and stable hydrogen evolution.

2. Experimental section

2.1 Preparation

The graphitic C_3N_4 (g-C_3N_4) nanosheets were synthesized by a modified thermal oxidation etching method using thiourea as the starting material.[29,30] Briefly, thiourea (Sinopharm, > 99%) was heated at 550 ^oC for 2 h in static air at a ramp rate of 2 ^oC/min. The resultant yellow bulk g-C_3N_4 was milled into fine powers. After that, 400 mg of bulk g-C_3N_4 was placed in an open ceramic container and then heated at 500 ^oC for 2 h at a ramp rate of 2 ^oC/min. Finally, a light yellow power of g-C_3N_4 nanosheets was obtained. The image could be found in Electronic Supplementary Information (ESI) Fig. S1.

The g-C_3N_4 nanosheets based MoS_2 composite photocatalysts were prepared by a photodeposition method in catalytic H_2 evolution. In this process, ammonium tetrathiomolybdate ($(NH_4)_2[MoS_4]$) were necessarily added as the resource of MoS_2. The deposition content of MoS_2 can be varied by changing the amount of $(NH_4)_2[MoS_4]$. The resultant products were denoted as g-C_3N_4/MoS_2-X (X = 0.75%, 1.47%, 2.18%, 2.89% and 3.57%), where X referred to the theoretical weight percent of loading MoS_2.

2.2 Characterization

X-ray diffraction (XRD) patterns were recorded on a D8 X-ray diffractometer (Bruker AXS, German). Transmission electron microscopy (TEM) image was collected on a JEM-2100 transmission electron microscope (JEOL, Japan). Energy-dispersive X-ray spectroscopy (EDX) was taken on the TEM. Fourier Transform infrared (FTIR) spectra were recorded over the 4000~800 cm^{-1} range by averaging 32 scans with a resolution of 4 cm^{-1} using a Nicolet 6700 (Thermal, USA) infrared spectrometer with a DLaTGS detector. Raman spectra were recorded on a confocal microscopic Raman spectrometer (Renishow In-Via, USA) with a 785 nm laser light irradiation from 200 to 1600 cm^{-1} at a duration time of 10 s. UV-vis diffuse reflectance spectra were measured on a UV-3600 (Shimadzu, Japan) spectrophotometer.

2.3 Photocatalytic hydrogen production

The photocatalytic experiments were performed in a 37 mL flask at ambient temperature using a 300 W Xe lamp equipped with UV cut off filter (λ > 400 nm). The intensity of the light source was estimated to be 0.6 W cm^{-2}. 10 mg of g-C_3N_4 nanosheets and a given amount of ammonium tetrathiomolybdate were added in a mixture solution of 9 mL water and 1 ml triethanolamine. Before each experiment, the suspension was purged with a nitrogen/methane gas mixture ($V_{nitrogen}$: $V_{methane}$ = 4 : 1) for 40 min to remove air. Methane served as the internal standard. Hydrogen gas evolution was measured by gas chromatography (SP-6890, nitrogen as a carrier gas) with a thermal conductivity detector (TCD).

2.4 Photoelectrochemical Measurement

A working electrode was prepared as follows: 20 mg of sample was dispersed in 4 mL water. 150 μL of the resultant suspension was uniformly droped onto a 1×1 cm^2 indium-tin oxide glass (ITO glass) and then dried at 70 °C for 1 h to obtain the working electrodes. Photocurrents were measured on a CHI600D electrochemical analyzer (Chenhua Instruments Co. Shanghai) in a standard three-electrode system by using the prepared electrode as the working electrode, a Pt net as the counter electrode, and Ag/AgCl as the reference electrode. A 300W Xe-lamp equipped with a band-glass light filter (> 400 nm) served as a light source. The electrolyte was a buffer solution (pH=6) containing 0.30 mol/L hexamethylenetetramine and 0.10 mol/L hydrochloric acid.

3 Results and discussion

3.1 Formation and characterization

In this work, the formation of MoS_2 resulted from the reduction of $(NH_4)_2[MoS_4]$ (equation 1), which were consistent with the previous literature.[31,32] Under visible light irradiation, g-C_3N_4 nanosheets adsorbed and harvested visible light to generate electrons and holes which were subsequently transported to the nanosheet surface. Due to high specific surface area of g-C_3N_4 nanosheet (260 m^2 g^{-1}), $[MoS_4]^{2-}$ can be effectively adsorbed on the g-C_3N_4 nanosheet surface. Photogenerated electrons in the g-C_3N_4 conduction band possessed enough reductive driving to reduce $[MoS_4]^{2-}$ precursor to MoS_2 + $2S^{2-}$,[24] leading to the production of g-C_3N_4/MoS_2 hybrid photocatalyst. On the other hand, the formative holes were scavenged by the sacrificial electron donor, such as triethanolamine. In this process, because the MoS_2 formed from the reduction of $[MoS_4]^{2-}$ by the photogenerated electrons, and then MoS_2 was in situ loaded on the electron outlet points of g-C_3N_4.

$$[MoS_4]^{2-} + 2e^- \rightarrow MoS_2 + 2S^{2-} \quad (1)$$

XRD was used to investigate the phase structure of the prepared pure g-C_3N_4 and hybrid g-C_3N_4/MoS_2 photocatalysts. Fig. 1 showed the XRD patterns of pure g-C_3N_4 nanosheets and g-C_3N_4/MoS_2 hybrid photocatalyst with different content of MoS_2. Both pure g-C_3N_4 and g-C_3N_4/MoS_2 had two distinct diffraction peaks at 28.0^o and 13.1^o which can be indexed to graphitic materials as the (002) and (100) planes of JCPDS

87-1526. These results illustrated that the g-C_3N_4 nanosheet structure maintained unchanged with MoS_2 modification. However, the diffraction intensity of peak at 28.0° became weaker with increasing MoS_2 content, which indicated that MoS_2 species to some extend restrained the growth of crystal structure of g-C_3N_4. No obvious MoS_2 peaks were observed from XRD patterns possibly due to the low content of MoS_2 and the well dispersed MoS_2 particles on g-C_3N_4 surface.

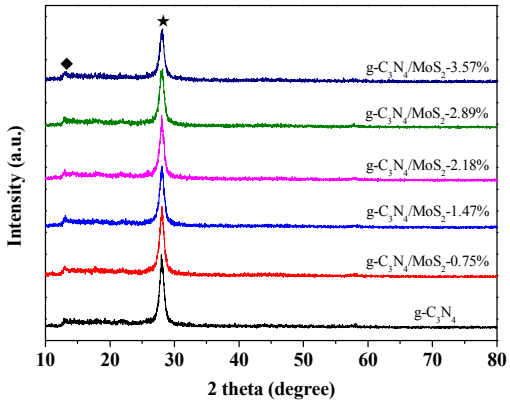

Fig. 1 XRD patterns of g-C_3N_4 and g-C_3N_4/MoS_2 with different MoS_2 contents.

FTIR spectra were used to study of chemical functional groups, and the result of pure g-C_3N_4 and g-C_3N_4/MoS_2-2.89% were presented in Fig. 2. The broad band located in 3100-3300 cm^{-1} involving residual N-H components and O-H bands were associated with uncondensed amino groups and surface-adsorbed H_2O molecures. A broad adsorption band in the region between 900 and 1800 cm^{-1} was related to the ploycondensation structure of g-C_3N_4 which were attributed to the vibration characteristic of s-striazine ring units and heptazine heterocyclic ring units.[33] Both pure g-C_3N_4 and g-C_3N_4/MoS_2-2.89% had similar absorption bands which indicated that the introduction of MoS_2 did not change the structure of g-C_3N_4 nanosheet structure. There was no MoS_2 peak was detected according to IR spectra. These results were in good accordance with XRD analysis.

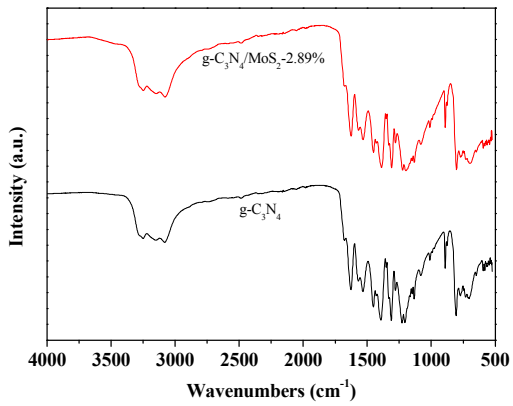

Fig. 2 IR spectra of g-C_3N_4 and g-C_3N_4/MoS_2-2.89%.

As depicted in Fig. 3, Raman spectroscopy was performed for the investigation of vibrational properties of pure g-C_3N_4 and g-C_3N_4/MoS_2-2.89%. Both pure g-C_3N_4 and g-C_3N_4/MoS_2-2.89% had the similar Raman bands mainly corresponding to surface defects and disorders located at the edges of graphite platelets.[34] However, the intensity of these peaks for g-C_3N_4/MoS_2-2.89% increased, which was attributed to eliminated surface defects of g-C_3N_4 after MoS_2 modification.[35] In comparison with Raman bands of pure g-C_3N_4, two new Raman bands at 392 cm^{-1} and 407 cm^{-1} appeared for g-C_3N_4/MoS_2-2.89%, which can be assigned to the representative modes of E_{2g}^1 and A_{1g} of MoS_2, respectively.[36] These results indicated the formation of MoS_2 on g-C_3N_4 surface.

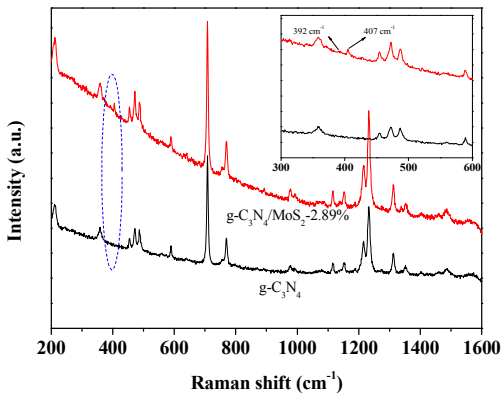

Fig. 3 Raman spectra of g-C_3N_4 and g-C_3N_4/MoS_2-2.89%.

TEM and EDX were used to observe the morphology and composition of g-C_3N_4/MoS_2-2.89% photocatalytst, and the results were given in Fig. 4. MoS_2 particles with size of several nanometers were deposited on the surface of g-C_3N_4 nanosheets (Fig. 4a). According to EDX patterns (Fig. 4b), C, N, Mo and S were observed (The Cu signal resulted from Cu grid for TEM characterization), and the EDX analysis results showed that the atomic ratio of S and Mo was about 2. These results further confirmed the uniformly deposition of MoS_2 particles on the surface by such in situ photoreduction method.

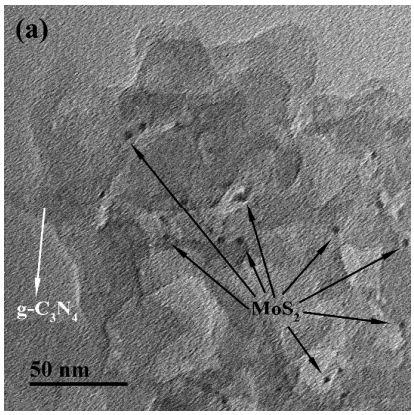

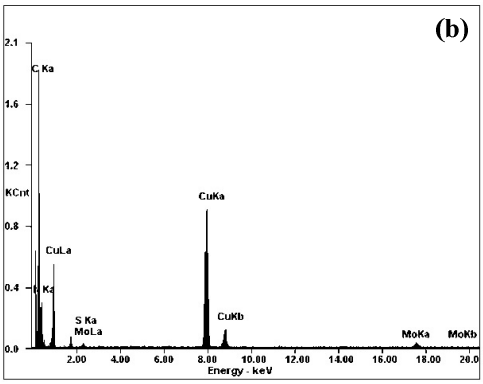

Fig. 4 TEM image (a) and EDX spectrum (b) of g-C_3N_4/MoS_2-2.89%.

The UV-vis diffuse reflection spectra of pure g-C_3N_4 and g-C_3N_4/MoS_2 with different MoS_2 contents were recorded in Fig. 5. As shown, the pure g-C_3N_4 had an absorption edge at about 450 nm which corresponded to a band gap of 2.71 eV. When MoS_2 was introduced, the g-C_3N_4/MoS_2 showed the same absorption edge as pure g-C_3N_4 indicating neither Mo nor S doping in the g-C_3N_4 structure. However, in comparison with pure g-C_3N_4, a broader absorption in the visible region was observed for g-C_3N_4/MoS_2 composite. Obviously, the absorption intensity for g-C_3N_4/MoS_2 in the visible region strengthened as the content of MoS_2 increased. Based on the XRD, Raman, TEM, EDX and DRS results, we can draw a conclusion that MoS_2 was deposited on the g-C_3N_4 surface by such a photoreduction method.

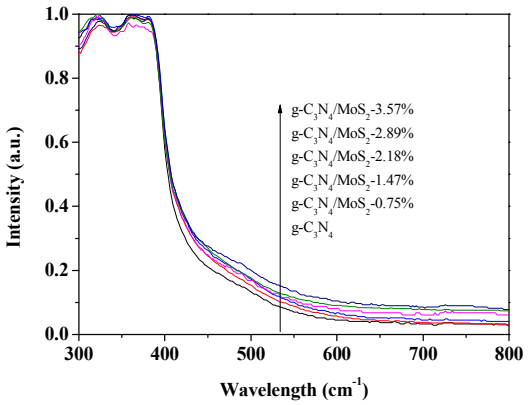

Fig. 5 UV-vis-diffuse reflection spectra of pure g-C_3N_4 and g-C_3N_4/MoS_2 with different MoS_2 contents.

3.2 Photocatalytic H_2 production

Fig. 6a showed the photocatalytic H_2 production activity of typical g-C_3N_4/MoS_2-2.89%. The H_2 production enhanced with the increase of irradiation time. During 6 h, the corresponding H_2 evolution was 1514 μmol g^{-1}. For comparison, the H_2 evolution activities for g-C_3N_4/MoS_2 with different MoS_2 loadings were investigated (Fig. 6b). When g-C_3N_4 alone was used as photocatalyst for H_2 evolution, the photocatlytic H_2 production rate was negligible because of fast recombination of photogenerated electrons and holes. These results indicated that pure g-C_3N_4 was not active for photocatalytic H_2 evolution and that MoS_2 was an effective cocatalyst for g-C_3N_4. As the content of MoS_2 loading increased from 0.75 wt% to 2.89 wt%, the H_2 evolution rate increased from 56 μmol g^{-1} h^{-1} to 252 μmol g^{-1} h^{-1}. However, the H_2 evolution activity for g-C_3N_4/MoS_2 decreased with further increasing MoS_2 loading content, which was possibly due to the overloading MoS_2 reducing oxidation reaction sites on g-C_3N_4 surface.[37]

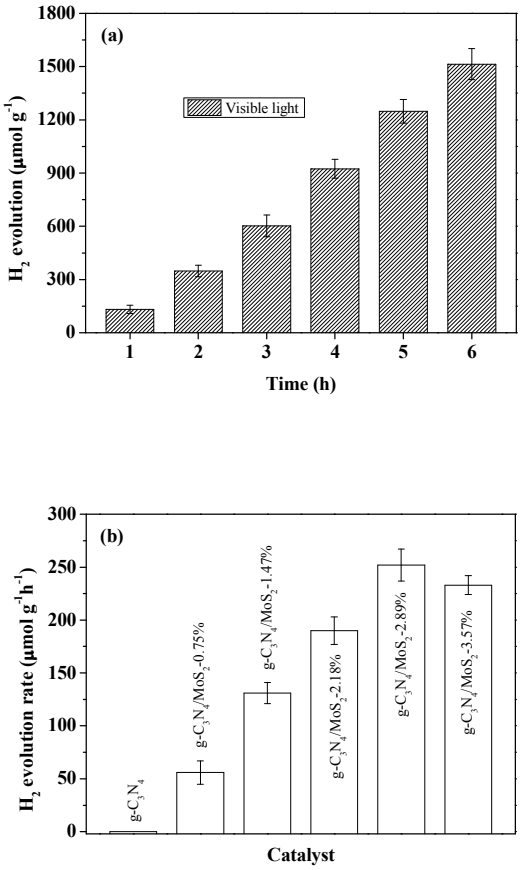

Fig. 6 (a) Photocatalytic hydrogen production over sample g-C_3N_4/MoS_2-2.89% during 6 h; (b) Comparison of photocatalytic hydrogen production rate over pure g-C_3N_4 and g-C_3N_4/MoS_2 with different MoS_2 contents.

The ultimate goal of photocatalyst is capable of high-efficiency application of sunlight and solar energy. Therefore, H_2 evolution was also conducted with g-C_3N_4/MoS_2-2.89% photocatalyst under direct sunlight outdoors (ESI Fig. S2). As illustrated in Fig. 7, the H_2 production increased with the prolongation of sunlight irradiation time. During 6 h, the H_2 evolution reached 1921 μmol g^{-1}, which was higher than that under visible light irradiation from Xe lamp. These results indicated that g-C_3N_4/MoS_2-2.89% was also a robust catalyst for sunlight-driven H_2 evolution from water. Such heterostructure may be expected to be promising candidates as effective sunlight photocatalysts and potential technological applications.

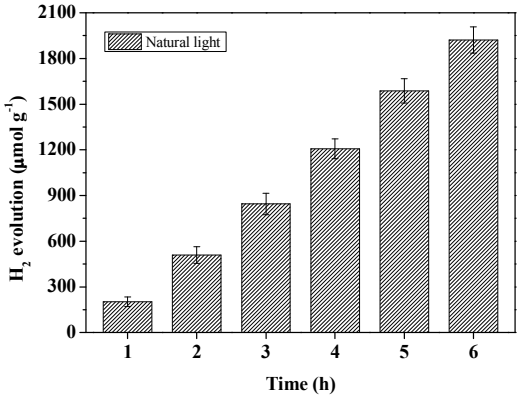

Fig. 7 Photocatalytic hydrogen production over g-C_3N_4/MoS_2-2.89% during 6 h under sunlight irradiation in Wuxi city on Nov. 18 2014. Outdoor temperature: 9-14 ºC, Time: 09:00- 15:00.

In view of practical applications, besides catalytic activity, the stability and durability are also indispensable to photocatalysts. In order to evaluate the stability of g-C_3N_4/MoS_2-2.89%, we performed the time-circle H_2 evolution experiment. Fig. 8 presented the H_2 evolution as the function of irradiation time. The total photocatalytic H_2 amount of g-C_3N_4/MoS_2-2.89% after 18 h reaction is about 4509 μmol g^{-1}. No noticeable degradation of photocatalytic H_2 evolution was detected in three repeated runs for the whole photocatalytic reaction, indicating the good stability and durability of the g-C_3N_4/MoS_2-2.89% sample. The results illustrated that the prepared g-C_3N_4/MoS_2-2.89% was an stable catalyst for photocatalytic H_2 evolution from water.

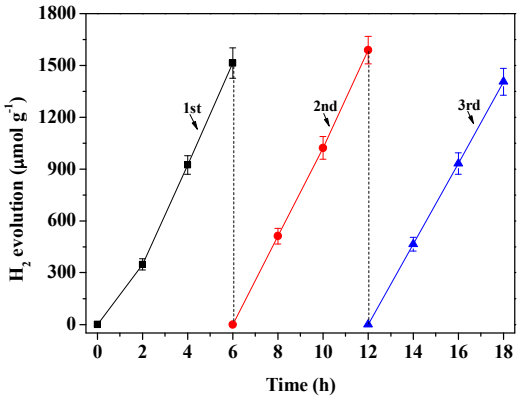

Fig. 8 Photocatalytic hydrogen production over g-C_3N_4/MoS_2-2.89% during 18 h with evacuation every 6 h.

3.3 Mechanism

Fig. 9 presented the proposed phtocatalytic H_2 production mechanism in g-C_3N_4/MoS_2 composite system. Under visible light irradiation, g-C_3N_4 was excited, the electrons and holes then generated. However, in pure g-C_3N_4, the photogenerated electrons and holes tended to recombine. After the modification of MoS_2 cocatalyst, the photogenerted electrons in conduction band of g-C_3N_4 can be easily transferred to the MoS_2. The unsaturated active S atoms existed on exposed edges of MoS_2 and had strong bonds to H^+ in the solution.[38] The trapped electrons at MoS_2 can easily reduce the bonded H^+, leading to H_2 generation (equation 2). As a result, the recombination of photogenerated electrons and holes on g-C_3N_4 was prevented obviously. To verify the proposed mechanism, photoluminescence (PL) emission spectra and photoelectrochemical (PEC) I-t curves were performed to study the charge recombination and transfer behavior of the g-C_3N_4/MoS_2 composite. Fig. 10a gave the PL spectra of pure g-C_3N_4 and g-C_3N_4/MoS_2-2.89% with an excitation wavelength of 325 nm. Both pure g-C_3N_4 and g-C_3N_4/MoS_2-2.89% showed an emission peak at about 455 nm corresponding to the band gap for the recombination of photogenerated electrons and holes.[39] However, the PL emission intensity of g-C_3N_4 obviously decreased after loading MoS_2, suggesting that the charge recombination can be efficiently prevented by MoS_2 modification. Figure 10b presented the PEC I-t curves of pure g-C_3N_4 and g-C_3N_4/MoS_2-2.89% electrodes under intermittent visible light irradiation at -0.22 V vs Ag/AgCl. Compared with pure g-C_3N_4, g-C_3N_4/MoS_2-2.89% hybrid photocatalyst showed the higher photocurrent density, which indicated the efficient photogenerated charge transfer between MoS_2 and g-C_3N_4 for g-C_3N_4/MoS_2-2.89%. These results confirmed the superior charge transfer and recombination inhibition in the g-C_3N_4/MoS_2-2.89% composite photocatalyst which supported the proposed mechanism.

$MoS_2/2H^+ + 2e^- \rightarrow MoS_2 + H_2$ (2)

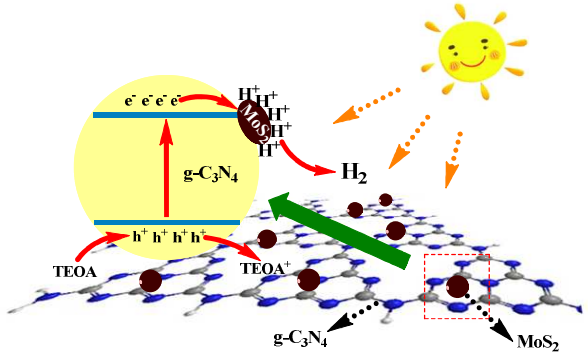

Fig. 9 Proposed photocatalytic H_2 production mechanism in the g-C_3N_4/MoS_2-2.89% composite systems under visible light irradiation.

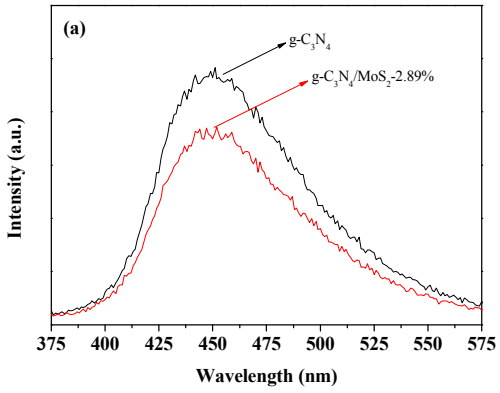

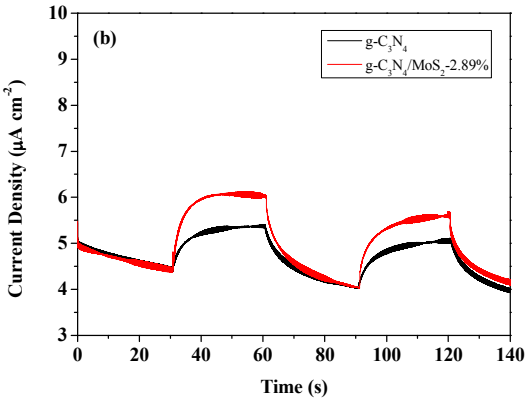

Fig. 10 Comparison of photoluminescence spectra (a) and transient photocurrent responses at -0.22 V vs Ag/AgCl (b) of pure g-C_3N_4 and g-C_3N_4/MoS_2-2.89%.

Conclusions

In conclusion, a novel preparation strategy for g-C_3N_4/MoS_2 hybrid photocatalysts was designed and realized by a simple and scalable in situ light-assisted method in photocatalytic H_2 evolution process. The photocatalytic H_2 evolution activity for g-C_3N_4 was significantly enhanced after MoS_2 cocatalyst loading. The highest H_2 evolution activity was determined for sample g-C_3N_4/MoS_2-2.89%, and the corresponding H_2 evolution rate was 252 μmol g^{-1} h^{-1}. In addition, g-C_3N_4/MoS_2-2.89% presented stable photocatalytic H_2 evolution ability and good natural light driven H_2 evolution ability. MoS_2 cocatalyst can efficiently promote the separation of photogenerated electrons and holes of g-C_3N_4 and consequently enhanced the H_2 evolution activity. The work may be significant to provide an insight into preparing g-C_3N_4 based hybrid photocatalytic materials with high activities for application in solar energy utilization and conversion.

Acknowledgement

The authors gratefully acknowledge the support from the National Natural Science Foundation of China (No. 20903048, 21275065), the Fundamental Research Funds for the Central Universities (JUSRP51314B and JUDCF13015), the Postgraduate Innovation Project of Jiangsu Province (CXZZ13-0743) and MOE & SAFEA for the 111 Project (B13025).

Notes and references

Key Laboratory of Food Colloids and Biotechnology (Ministry of Education of China), School of Chemical and Material Engineering, Jiangnan University, Wuxi 214122, P. R. China. Fax: (+) 86-510-85917763; E-mail: dongym@jiangnan.edu.cn, ppjiang@jiangnan.edu.cn

† Electronic Supplementary Information (ESI) available: [details of any supplementary information available should be included here]. See DOI: 10.1039/b000000x/

1 Z. B. Yu, Y. P. Xie, G. Liu, G. Q. (Max) Lu, X. L. Ma, and H. -M. Cheng, J. Mater. Chem. A, 2013, 1 , 2773-2776.
2 Q. Wang, J. Li, Y. Bai, J. Lian, H. Huang, Z. Li, Z. Lei and W. Shangguan, Green Chem., 2014, 16, 2728-2735.
3 Y. P. Xie, Z. B. Yu, Gang Liu, X. L. Ma, and H. -M. Cheng, Energy Environ. Sci., 2014, 7, 1895-1901.
4 X. B. Chen, S. S. Mao, Chem. Rev., 2007, 107, 2891-2959.
5 X. B. Chen, S. H. Shen, L. J. Guo, S. S. Mao, Chem. Rev., 2010, 110, 6503-6570.
6 D. -H. Wang, L. Wang and A. -W. Xu, Nanoscale, 2012, 4, 2046-2053.
7 J. Zhang, X. Chen, K. Takanabe, K. Maeda, K. Domen, J. D. Epping, X. Fu, M. Antonietti, and X. Wang, Angew. Chem. Int. Ed., 2010, 49, 441-444.
8 Y. Wang, X. Wang, and M. Antonietti, Angew. Chem. Int. Ed., 2012, 51, 68-89.
9 X. Wang, S. Blechert, and M. Antonietti, ACS Catal., 2012, 2, 1596-1606.
10 J. Chen, S. Shen, P. Guo, M. Wang, P. Wu, X. Wang, and L. Guo, Appl. Catal. B: Environ., 2014, 152-153, 335-341.
11 L. Ge, C. Han, and J. Liu, J. Mater. Chem., 2012, 22, 11843-11850.
12 L. Ge, C. Han, X. Xiao, and L. Guo, Appl. Catal. B: Environ., 2013, 142-143, 414-422.
13 C. Han, L. Ge, C. Chen, Y. Li, X. Xiao, Y. Zhang, and L. Guo, Appl. Catal. B: Environ., 2014, 147, 546-553.
14 X. Bai, L. Wang, Y. Wang, W. Yao, and Y. Zhu, Appl. Catal. B: Environ., 2014, 152-153, 262-270.
15 S. Cao, and Jiaguo Yu, J. Phys. Chem. Lett., 2014, 5, 2101-2107.
16 S. Zhang, J. Li, M. Zeng, J. Li, J. Xu, and X. Wang, Chem. Eur. J., 2014, 20, 9805-9812.
17 D. J. Martin, K. Qiu, S. A. Shevlin, A. D. Handoko, X. Chen, Z. Guo, and J. Tang, Angew. Chem. Int. Ed., 2014, 53, 9240-9245.
18 K. Maeda, X. C. Wang, Y. Nishihara, D. Lu, M. Antonietti, K. Domen, J. Phys. Chem. C, 2009, 113, 4940-4947.
19 Y. Di, X. C. Wang, A. Thomas, M. Antonietti, ChemCatChem, 2010, 2, 834-838.
20 J. Xie, J. Zhang, S. Li, F. Grote, X. Zhang, H. Zhang, R. Wang, Y. Lei, B. Pan, and Y. Xie, J. Am. Chem. Soc., 2013, 135, 17881-17888.
21 J. Xie, H. Zhang, S. Li, R. Wang, X. Sun, M. Zhou, J. Zhou, X. W. (David) Lou, and Y. Xie, Adv. Mater., 2013, 25, 5807-5813.
22 X. Zong, H. Yan, G. Wu, G. Ma, F. Wen, L. Wang and C. Li, J. Am. Chem. Soc., 2008, 130, 7176-7177.
23 Q. Xiang, J. Yu, and M. Jaroniec, J. Am. Chem. Soc., 2012, 134, 6575-6578.
24 M. Nguyen, P. D. Tran, S. S. Pramana, R. L. Lee, S. K. Batabyal, Nanoscale, 2013, 5, 1479-1482.
25 Y. Hou, A. B. Laursen, J. Zhang, G. Zhang, Y. Zhu, X. Wang, S. Dahl, and I. Chorkendorff, Angew. Chem. 2013, 125, 3709-3713; Angew. Chem. Int . Ed. 2013, 52, 3621-3625.
26 L. Ge, C. Han, X. Xiao, and L. Guo, Int. J. Hydrogen Energy, 2013, 38, 6960-6969.
27 Y. Tian, L. Ge, K. Wang, and Y. Chai, Mater. Charter., 2014, 87, 70-73.
28 W. Peng, and X. Li, Catal. Commun., 2014, 49, 63-67.
29 P. Niu, L. Zhang, G. Liu, and H. -M. Cheng, Adv. Funct. Mater., 2012, 22, 4763-4770.
30 W. Wang, J. C. Yu, D. Xia, P. K. Wong, and Y. Li, Environ. Sci. Technol., 2013, 47, 8724-8732.
31 L. Liao, J. Zhu, X. Bian, L. Zhu, M. D. Scanlon, H. H. Girault, and B. Liu, Adv. Funct. Mater., 2013, 23, 5326-5333.
32 X. Bian, J. Zhu, L. Liao, M. D. Scanlon, P. Ge, C. Ji, H. H. Girault, B. Liu, Electrochem. Commun., 2012, 22, 128-132.
33 J. R. Holst, and E. G. Gillan, J. Am. Chem. Soc., 2008, 130, 7373-7379.
34 G. X. Wang, X. P. Shen, J. Yao, and J. Park, Carbon, 2009, 47, 2049-2053.
35 X. Bai, L. Wang, R. Zong, and Y. Zhu, J. Phys. Chem. C, 2013, 117, 9952-9961.
36 M. Shen, Z. Yan, L. Yang, P. Du, J. Zhang, and B. Xiang, Chem. Commun., 2014, 50, 15447-15449.
37 X. Wang, G. Liu, Z. -G. Chen, F. Li, L. Wang, G. Q. Lu, and H. -M. Cheng, Chem. Commun., 2009, 3452-3454.
38 K. Chang, Z. Mei, T. Wang, Q. Kang, S. Ouyang, and J. Ye, ACS NANO, 2014, 8, 7078-7087.
39 P. Gomathisankar, K. Hachisuka, H. Katsumata, T. Suzuki, K. Funasaka, and S. Kaneco, ACS Sustainable Chem. Eng., 2013, 1, 982-988.

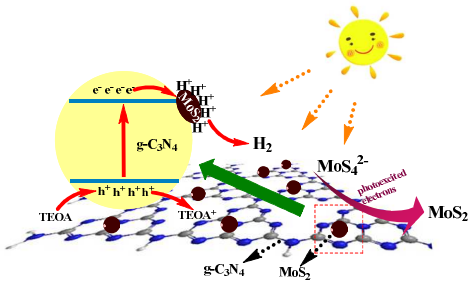	In situ photodeposition of MoS_2 on graphitic C_3N_4 surfaces for enhanced photocatalytic H_2 evolution from water